Challenges and Limitations of Terahertz Phase Imaging Method

Mateusz Kaluza,[*1] Adrianna Nieradka,[1] Paweł Komorowski,[2] and Agnieszka Siemion[1]

[1]*Faculty of Physics, Warsaw University of Technology, Koszykowa 75, 00-662 Warsaw, Poland*
[2]*Institute of Optoelectronics, Military University of Technology, gen. S. Kaliskiego 2, 00-908 Warsaw, Poland*

Received December 15, 2024; accepted December 26, 2024; published December 31, 2024

Abstract—Advancements in terahertz (THz) technology have significantly enhanced imaging systems, while improving imaging contrast remains critical, especially for transparent objects. This study presents a 4f imaging system using the positive phase contrast method, tested on a transparent 3D-printed object with varying phase retardations. Parasitic effects observed during experiments highlight key challenges in THz imaging, enabling the identification of solutions to improve system performance and enhance image quality.

In optics, imaging techniques utilizing spatial filtering or polarized light are employed to enhance the contrast of examining transparent (low absorptive) objects. In the context of terahertz (THz) technology, imaging methods have numerous applications across various fields [1]. In medicine, they are used to distinguish specific tissue characteristics, such as differentiating water-induced absorption from potential structural changes in tissues [2-3]. This capability facilitates non-invasive diagnostics for various types of cancerous changes [4-5].

In security systems, THz imaging techniques are applied to detect hazardous hidden objects and explosive materials [6-7]. Furthermore, in industry, THz imaging enables non-invasive testing of products, such as identifying defects like delaminations in objects [8-9]. Notable imaging techniques include dark-field (DF) method [10], homodyne imaging [11], as well as positive phase-contrast (PPC) and negative phase-contrast (NPC) approaches [12].

However, it should be noted that THz radiation is characterized by relatively long wavelengths. Thus, optical imaging systems operate in the near-field zone, also referred to as the Fresnel diffraction zone. Furthermore, THz radiation sources used in imaging systems, such as Resonant Tunnelling Diodes (RTD), Schottky diode-based mixer-amplifier-multiplier chains (e.g., those produced by Virginia Diodes Inc. (VDI)), or Impact Ionization Avalanche Transit-Time (IMPATT) diodes, are exceptionally coherent [13]. This feature contributes to significant challenges in THz imaging systems, such as various parasitic interference effects.

In this study, we present a 4f THz imaging setup employing the PPC method, which enables the imaging of transparent objects by applying the phase filter, introducing a phase shift of $\pi/2$ in the Fourier plane. The study puts particular emphasis on addressing the challenges posed by THz imaging and on methods that can be implemented to mitigate undesirable THz radiation interferences arising in such systems. The scheme of the 4f imaging system utilizing the PPC method is presented in Fig. 1.

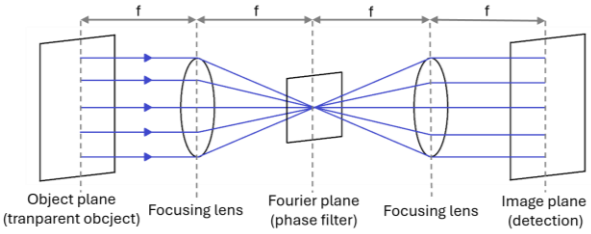

Fig. 1. The scheme of the 4f imaging system utilizing the phase-contrast method. It consists of two focusing lenses and a phase filter between them.

When considering the 4f system with phase contrast filtering (Fig. 1), the object to be imaged is placed in the object plane and is illuminated by a monochromatic quasi-plane wave. Next, a focusing lens is positioned within the system at a focal distance f from the object plane. This lens performs the Fourier transform of the incoming wavefront.

At the distance of focal length f behind the focusing lens (in the Fourier plane), a spatial phase filter is placed, introducing a certain phase delay for low spatial frequencies. Introduced phase delay enables modification of the original spectral distribution of the object by enhancing variations in the object's phase distribution. Subsequently, another focusing lens, positioned at the focal distance f from the Fourier plane, performs the Fourier transform again. As a result, an inverted (in both directions) image of the object with enhanced contrast, highlighting the phase variations of the investigated object, is formed at a distance of four focal lengths (which in our system was equal to 1200 mm) from the object plane.

This study investigated an object with a circular aperture of 200 mm in diameter for a frequency of 140 GHz (wavelength of 2.141 mm). The object was a phase element designed as a grayscale map with pixel values ranging from 0 to 255 and represented phase delays introduced by the object, ranging from 0 to $\pi/2$. The object consisted of seven letters forming the word

* E-mail: mateusz.kaluza.dokt@pw.edu.pl

"PHYSICS," each letter introducing a different phase delay. Figure 2a shows the phase distribution map of the object.

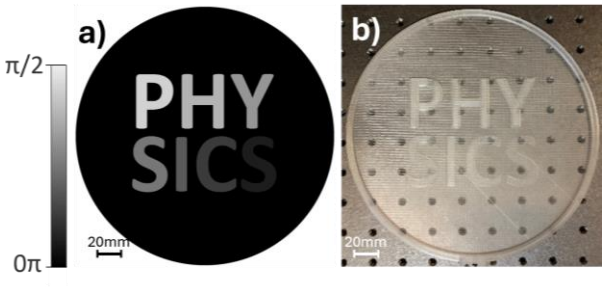

Fig. 2. The object investigated in the 4f imaging system: a) grayscale bitmap of the object corresponding to the phase distribution; b) 3D-printed structure fabricated using FDM technology with COC material.

Based on the obtained bitmap, a 3D model of the object was created and had the thickness of particular segments according to Eq. (1):

$$h(x,y) = \frac{\phi(x,y)}{0.5\pi} \cdot \frac{\lambda}{n - n_0}, \tag{1}$$

where $h(x,y)$ represents the pixel values (heights/ thickness) of the structure introducing phase delay $\phi(x,y)$, λ is the considered wavelength, n is the refractive index of the manufactured structure's material, and n_0 is the refractive index of the surrounding medium (typically equal to 1 for the air).

The spatial structure representing the object was fabricated using 3D printing fused deposition modeling (FDM) technology with cyclic olefin copolymer (COC) filament provided by Creamelt. COC is a material characterized by an exceptionally low absorption coefficient and a refractive index approximately equal to 1.5 in the THz radiation range [14]. Additionally, a substrate with a thickness of 500 μm was introduced to support the object elements and ensure the stability as well as the rigidity of the structure under investigation. The substrate introduced constant phase delay in the whole area of the structure. Thus, it should not significantly affect the results of the experiment. All 3D-printed elements in this study were manufactured using the Prusa i3 MK3S+ printer, providing a horizontal accuracy of 12 μm and a vertical accuracy of 2 μm. The prints were produced with a line width of 450 μm and a layer thickness of 100 μm, respectively, determining the prints' horizontal and vertical resolution.

A photograph of the 3D-printed structure is presented in Fig. 2b, while Table 1 provides the phase delays introduced by each segment (letter) of the object, which depends on their corresponding thicknesses.

Table 1. The height of the manufactured segments (substrate thickness not included) of the structure and the corresponding phase delay introduced by different segments of the structure.

The segments of the object	Hight of the segment	Introduced phase delay
"P"	1.1 mm	0.50π
"H"	0.9 mm	0.41π
"Y"	0.8 mm	0.36π
"S"	0.6 mm	0.27π
"I"	0.5 mm	0.23π
"C"	0.3 mm	0.14π
"S"	0.2 mm	0.09π

In the first stage, the imaging of the proposed object was evaluated through numerical simulations, following the scheme shown in Fig. 1. For this purpose, the LightSword 6.0 software by Orteh, based on a modified convolution method, was utilized. The numerical simulations employed the phase delay map shown in Fig. 2a as the object, two kinoform lenses with focal lengths of 300 mm, and a phase filter with a 7 mm diameter, introducing a phase delay of π/2. Fig.a presents the simulation results without the phase filter, while Fig. 3b shows the results obtained with the phase filter applied in the Fourier plane.

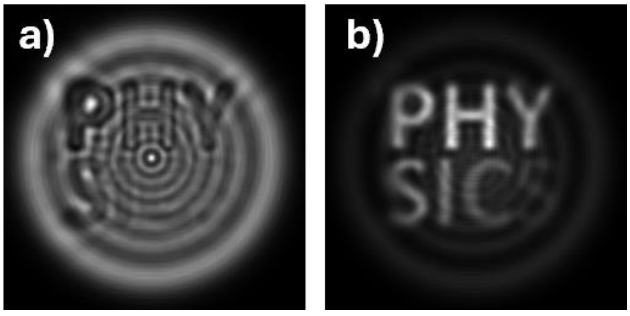

Fig. 3. Intensity distributions obtained from numerical simulations performed using the modified convolution method: a) intensity distribution in the image plane without the phase contrast filter applied; b) intensity distribution in the image plane with the phase contrast filter applied.

The obtained numerical simulation results clearly demonstrate a significant improvement in the contrast for imaging transparent objects in the THz range when the PPC is applied. However, particular attention should be paid to the undesired effect of diffraction resulting from the finite aperture size that is related to Fresnel zones in the output field distribution (intensity distribution in the image plane) resulting from operation in the near-field region. In experimental conditions, this effect may be further amplified by unwanted interferences, which are unavoidable in THz optical systems employing coherent radiation sources.

Subsequently, the manufactured structure was examined in the 4f experimental THz setup with the applied PPC method. Figure 4 presents a photograph of

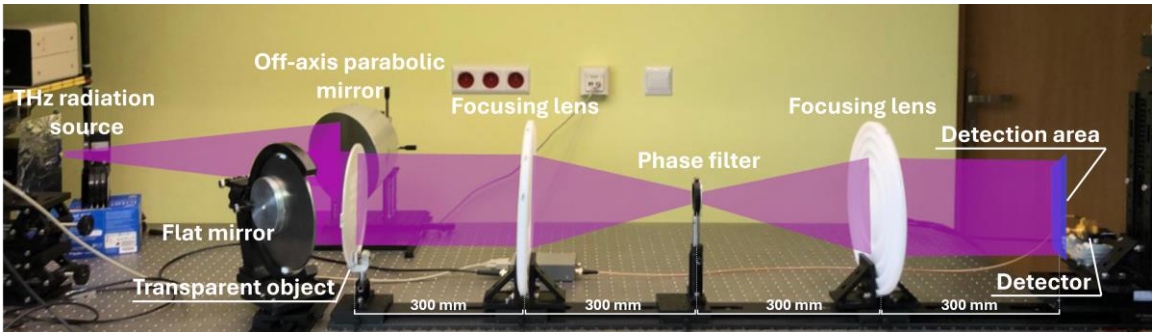

Fig. 4. Photograph of the experimental setup for the THz PPC method implemented in the 4f system.

the setup with a visualization of the optical paths of the THz beam.

In the experimental setup shown in **Błąd! Nie można odnaleźć źródła odwołania.**4, a VDI frequency multiplier was used to generate monochromatic THz radiation with a dominantly Gaussian beam profile at a frequency of 140 GHz. The radiation illuminated an off-axis parabolic mirror, which shaped the beam into a quasi-planar wavefront. A flat mirror then redirected the beam to the object located in the input of the 4f optical system.

At the input of the 4f system, a 3D-printed transparent structure for THz radiation was placed, with segments introducing varying phase delays. At a distance of 300 mm, a converging lens with a diameter of 300 mm and a focal length of 300 mm was positioned to act as the focusing element. The converging lens was produced using the milling method. Its design and manufacturing process were described in detail in a previous study [15].

A phase filter was introduced in the Fourier plane, located 300 mm from the converging lens. The phase filter was manufactured using FDM 3D printing technology from COC similarly to the investigated object. It had a cylindrical shape with a diameter of 7 mm and a thickness of 1.1 mm. Another converging lens with the same parameters [15] was placed at a distance of 300 mm, completing the passive elements of the 4f system.

Finally, a vertical field scan at the image plane, located 300 mm beyond the second lens, was performed using a VDI detector mounted on motorized *xyz* translation stages. The vertical scan was conducted with a step size of 2 mm. The voltage U, measured by the detector, is directly proportional to the intensity of THz radiation in the image plane. The normalized intensity distribution obtained experimentally in the image plane compared with the simulation results is presented in Fig. 5 (linear interpolation applied).

The experimental results presented in Fig. 5b demonstrate the successful implementation of imaging using the PPC method. The segments of the imaged object "P," "H," and "Y" are distinctly visible and stand out from the surrounding background.

However, the segments in the structure's "second row" are not clearly discernible in the acquired scan, which is expected due to the introduced smaller phase shift value.

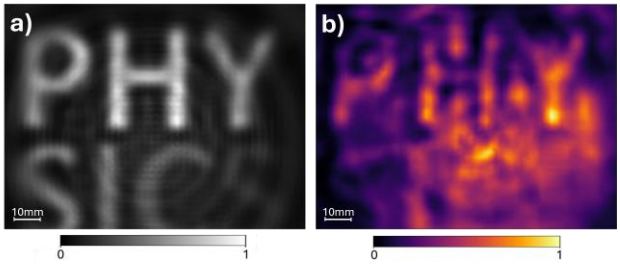

Fig. 5. The reconstructed image of the transparent object in the 4f THz system with the phase contrast method: a) numerical simulation results; b) experimental results.

Firstly, subsequent segments introduce progressively smaller phase delays. The phase contrast filter operates properly for particular phase delays introduced by the object – being in the range from 0 to $\pi/2$. For larger phase delays, a phase contrast method stops functioning properly, and it does not maintain the linear dependence of the phase delay of the object with the intensity profile at the image plane.

Additionally, the registered intensity patterns reveal significant interference effects caused by multiple reflections of the coherent THz radiation within the system and inside the object. As noted earlier in this study, the near-field operation of the system and the large coherence of sources introduce additional interference effects.

Due to the observed interference effects in the recorded signal, more detailed measurements were conducted. Linear scans of the image plane field were performed twice across each row of the object's segments in a setup without a phase filter. Equivalent scans were also conducted in the setup without the object to determine the reference voltage U_0 registered by the detector. The results of the two scans were then averaged for each case.

Figure 6a illustrates the scan range for the first row of segments, marked with a red line. Meanwhile, Fig. 6b presents the difference in the recorded signal with and without the object $(U-U_0)$ as a function of the horizontal x position.

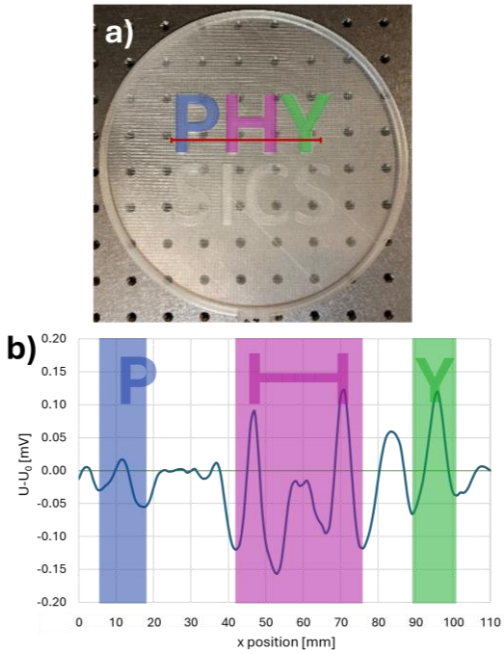

Fig. 6. a) 3D-printed structure with marked range of the scan performed for the first row of letters. b) Experimentally registered values showing the difference in the recorded signal for the marked range of the scan.

In Fig. 6b, notable variations in the recorded signal amplitude within the segment areas corresponding to different phase values of the object can be observed. However, the measurement results clearly indicate the presence of significant interference effects being present in the system due to the particular shape of the sample. The signal recorded during measurements of the investigated structure is, in several areas, significantly higher than the reference signal (measured without the object). This is particularly evident for the "H" and "Y" segments. This effect might arise from the geometry of the investigated object, which is planar and parallel. Such a configuration leads to internal Fresnel reflections and, consequently, a resonator effect, which in this case is parasitic. The scheme of the parasitic Fresnel reflection effect is presented in Fig. 7.

When considering a flat and parallel object, the radiation undergoes multiple internal reflections within the structure. As a result, in addition to the signal directly transmitted through the sample, characterized by an amplitude A_1 and phase ϕ_1, there is a contribution from internally reflected radiation with an amplitude A_2 and phase ϕ_2 (for simplicity, only the first internal reflection is considered). The signal detected by the system is a superposition of these two components, with its intensity I_{RES} described by Eq. (2). Consequently, constructive interference occurs when the signals are in phase, leading to an enhanced detected signal:

$$I_{RES} = |A_{RES}|^2 = |A_1|^2 + |A_2|^2 + 2A_1A_2\cos(\Delta\phi), \qquad (2)$$

where I_{RES} represents the resulting intensity detected after interference, A_{RES} is the resultant amplitude of the combined waves, A_1 and A_2 are the amplitudes of the directly transmitted wave and the internally reflected wave, respectively, and $\Delta\phi$ is the phase difference between these two waves.

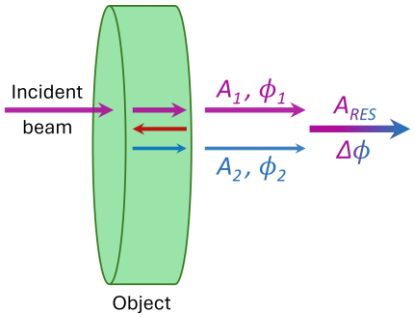

Fig. 7. Illustration of the parasitic Fresnel reflections occurring in flat, parallel-sided objects.

After conducting the analysis, a significant impact of Fresnel reflections was observed, which influenced the imaging of the transparent object, leading to variations in the recorded signals. As a result of the unexpected findings presented in Fig. 6, additional measurements were conducted. A segment corresponding to each letter was placed in the system at the same spatial position, and the corresponding signal U was recorded using the detector (the intensity registered after the object without using any filters). Additionally, measurements were performed for the signal transmitted through the substrate alone and for the reference signal without an object inserted into the setup. Table 2 summarizes the obtained results, including the phase difference $\Delta\phi$ between the signal transmitted through the object and the signal detected, taking into account the refractive index of the 3D-printed structure (n = 1.51).

Table 2. The local height of the structure's segments (substrate thickness included), the phase difference between the signal transmitted through the object and the reflected signal gathered by the detector, and the gathered signal by the detector.

The elements of the object	Local hight of the object	$\Delta\phi$	U
"P"	1.6 mm	4.51π	215 mV
"H"	1.4 mm	3.95π	245 mV
"Y"	1.3 mm	3.67π	228 mV
"S"	1.1 mm	3.10π	218 mV
"I"	1.0 mm	2.82π	203 mV
"C"	0.8 mm	2.26π	195 mV
"S"	0.7 mm	1.97π	192 mV
substrate	0.5 mm	1.41π	170 mV
reference	-	-	193 mV

The analysis of phase delay values and measured signals, as presented in Table 2, indicates that the proposed phase contrast method performs more effectively for thicker structures, which is an expected behavior. In these cases, the phase delay introduced by the filter enables the enhancement of contrast when

imaging the object. However, the majority of the recorded voltage values significantly exceed the reference signal measured in the absence of the filter. This finding highlights the considerable influence of Fresnel reflections inside the object on the final recorded signal values.

One of the most notable observations was the highest recorded signal of 245 mV corresponding to the segment "H", where the reflected beam was nearly in phase with the signal propagating through the structure to the detector.

It is also noteworthy that the COC used to fabricate the structures is highly transparent to THz radiation [14]. While its exceeding low absorption coefficient minimizes radiation attenuation, simultaneously, the impact of the parasitic Fresnel reflection and other interference effects within the optical system is more visible. Nonetheless, the use of a material that is as transparent as possible remains a critical factor in achieving reliable experimental results for phase contrast imaging techniques.

To address the challenges encountered during phase contrast imaging of transparent objects in the 4f system, several improvements are proposed to enhance system performance and data reliability. First, the experimental setup could benefit from the integration of apertures at each optical element. These apertures, fabricated from THz absorbing or reflecting materials such as carbon- or graphene-based composites [16], would significantly reduce unwanted off-axis interferences within the system. Additive manufacturing technologies, such as FDM, offer access to cost-efficient composites containing materials like polypropylene (PP), polycarbonate (PC), or polyethylene terephthalate glycol (PETG) infused with carbon fibers, which exhibit exceptional THz attenuation properties. Components manufactured from such materials could serve as effective optical shields.

Moreover, optimization of the geometry of the imaged objects is essential. Encasing the proposed segments in a transparent casting material with a refractive index distinct from that of the object could significantly reduce Fresnel reflections within the structure. Recent studies have demonstrated that materials like paraffins, which are transparent to THz radiation, can serve this purpose [17]. Alternatively, hybrid structures composed of materials with varying optical properties or objects designed with a gradient refractive index could be employed. Such designs would specifically address the challenges posed by Fresnel reflections during phase contrast imaging.

Finally, the limitations of plane-parallel objects in this context necessitate consideration of alternative spatial profiles. Objects encountered in practical applications often feature complex and varied geometries. Therefore, it is essential to investigate objects with more intricate shapes to better understand the performance of the imaging system under realistic conditions. However, it remains crucial to address and minimize undesired interference within the imaging system to ensure the reliability and accuracy of the results. Designing objects that introduce continuous phase changes would be more appropriate in the context of real-world applications.

These proposed modifications highlight the need for systematic refinement of the experimental approach. Future studies will explore these aspects to address the inherent challenges of THz imaging, particularly for transparent objects, and to enhance the reliability and accuracy of phase contrast imaging methods.

In conclusion, this study demonstrates the 4f system with a positive phase contrast filter and highlights the challenges in implementing such THz imaging setups. The plane-parallel object with segments introducing different phase delays was designed and fabricated using 3D printing in FDM technology, with a highly transparent COC selected for THz radiation. Experimental measurements confirmed the successful imaging of regions introducing higher phase changes.

However, detailed analysis revealed significant interference effects, primarily caused by parasitic Fresnel reflections within the plane-parallel object. To address these issues, proposed solutions include optimizing the geometry of the imaged structures, using casting methods, or developing hybrid designs. Shields made from low-cost carbon composites produced via additive manufacturing are also suggested. These approaches aim to improve imaging contrast and minimize parasitic interference, enhancing the system's overall performance.

Studies were funded by the FOTECH-1 project granted by Warsaw University of Technology under the program Excellence Initiative: Research University (ID-UB). The Authors would like to thank Orteh Company for providing LS 6.0 software used here for numerical simulations of spatial filtering methods, which is accessible in the Laboratory of Optical Information Processing at the Faculty of Physics at Warsaw University of Technology.

References

[1] D.M. Mittleman, Opt. Express **26**, 8 (2018).
[2] Z. Yan, L.G. Zhu, K. Meng, W. Huang, Q. Shi, Trends Biotechnol. **40**, 7 (2022).
[3] G.M. Png *et al.*, Phys. Med. Biol. **53**, 13 (2008).
[4] L. Wang, Sensors **21**, 19 (2021).
[5] Y. Peng, C. Shi, X. Wu, Y. Zhu, S. Zhuang, BME Front. **2020,** (2020).
[6] Y. Tzydynzhapov *et al.*, J. Infrared Millim. Terahertz Waves **41**, 6 (2022).
[7] A.G. Davies *et al.*, Mater. Today **11**, 3 (2008).
[8] S. Zhong, Front. Mech. Eng. **14**, 3 (2019).
[9] S. Fan *et al.*, AIP Adv. **7**, 11 (2017).
[10] T. Löffler *et al.*, Opt. Express **9**, 12 (2001).
[11] G. Valušis, A. Lisauskas, H. Yuan, W. Knap, H.G. Roskos, Sensors **21**, 12 (2021).
[12] F. Zernike, Z Tech Physik **16**, 454 (1935).
[13] I. Mehdi, J.V. Siles, C. Lee, E. Schlecht, Proc. IEEE **105**, 6 (2017).
[14] M. Kaluza, M. Walczakowski, A. Siemion, Materials **17**, 20 (2024).
[15] M. Sypek *et al.*, Opt. Lett. **37**, 12 (2012).
[16] K. Zeranska-Chudek, A. Lapinska, A. Siemion, A.M. Jastrzębska, M. Zdrojek, J. Appl. Polym. Sci. **138**, 10 (2021).
[17] A. Siemion, IEEE Trans. Terahertz Sci. Technol. **11**, 4 (2021).

